Journal of Magnetic Resonance 212 (2011) 197–203

Contents lists available at ScienceDirect

Journal of Magnetic Resonance

journal homepage: www.elsevier.com/locate/jmr

Standard-based method for proton–electron double resonance imaging of oxygen

Olga V. Efimova, George L. Caia, Ziqi Sun, Sergey Petryakov, Eric Kesselring, Alexandre Samouilov, Jay L. Zweier *

Davis Heart and Lung Research Institute and Division of Cardiovascular Medicine, Department of Internal Medicine, College of Medicine, The Ohio State University, Columbus, OH 43210, USA

ARTICLE INFO

Article history:
Received 16 May 2011
Revised 24 June 2011
Available online 2 July 2011

Keywords:
Functional MRI
Free radicals
Oximetry
Overhauser MRI
Trityl radical probes

ABSTRACT

Proton–electron double resonance imaging (PEDRI) has been utilized for indirect determination of oxygen concentrations in aqueous samples and living systems. Due to the complexity of the problem, there are seven oxygen related parameters that need to be measured to determine the distribution of oxygen. We present an improved approach in which image intensities from only two PEDRI acquisitions with different EPR irradiation powers are required to determine the distribution of a paramagnetic probe and oxygen in an analyzed sample. This is achieved using three reference samples with known concentrations of a paramagnetic probe and oxygen placed inside the resonator together with the measurement sample. An EPR-off image, which has low signal intensity at low magnetic field (0.02 T) is not required for the calculations, significantly reducing the total time of the experiments and the noise while enhancing the accuracy of these oxygen measurements. The Finland trityl radical was used as the paramagnetic probe and oxygen concentrations could be accurately measured and imaged over the physiological range from 0 to 240 μM.

Published by Elsevier Inc.

1. Introduction

The concentration of dissolved molecular oxygen in organs, tissues and cells of a living organism is directly affected by many physiological and pathophysiological processes. Therefore, to understand normal physiology and disease it is important to be able to accurately measure oxygen concentration. Invasive methods, for example, using oxygen sensitive electrodes, have many disadvantages, including the fact that the electrodes need to be placed directly in the tissue causing local injury. Their ability to absorb oxygen can also affect the accuracy of the measurements. Noninvasive methods are mostly based on magnetic resonance techniques, both spectroscopic and imaging. MRI methods have found many applications for oximetry measurements, including ^{19}F MRI oximetry and ^{1}H blood oxygen level-dependent MRI [1] but with relatively low sensitivity. Higher sensitivity to oxygen can be achieved using exogenous paramagnetic probes due to the presence of a single electron based substance [2–4]. Electron paramagnetic resonance imaging (EPRI) methods provide functional information but typically do not provide complementary anatomical structure as can be obtained with proton MRI.

Proton–electron double resonance imaging (PEDRI) is one of the promising noninvasive methods to indirectly measure the concentration of oxygen. In this technique, proton MRI is acquired while irradiating and saturating the electron spin system [5,6]. This double resonance technique couples the spatial resolution of MRI with the functional sensitivity of EPR. As a result, NMR signal intensity of the magnetically coupled water protons can be significantly increased in the regions where the paramagnetic probe is present. Enhancement of the nuclear polarization in solutions occurs via dipole – dipole interaction and depends on several factors, such as: (1) EPR spectral characteristic; (2) concentration of the paramagnetic probe; (3) relaxivity in the solution; (4) the electron relaxation times of the probe; and (5) applied RF power for EPR saturation. The term "relaxivity" refers to the ability of the probe to alter tissue relaxation rates, T_1^{-1} and T_2^{-1}, per probe unit concentration. This effect of spin polarization transfer, initially proposed by Overhauser [6], has found many applications since its discovery [5,7]. A special class of trityl radicals, tetrathiotriaryl methyl (TAM) radicals is very well suited for PEDRI experiments as they exhibit relatively long electron relaxation times and, therefore, a sharp single line EPR spectrum [8–14]. Low toxicity and good stability allow these probes to be used for in vitro as well as in vivo experiments [15].

A decade ago in vivo PEDRI was applied for determining the tissue oxygen status of small animals by several research groups [16,17]. It was found that two images acquired at different EPR irradiation powers and one EPR-off image are needed to determine the concentration of the probe and oxygen using the following equations [17]

$$C_R^{an} = \left\{1/E_{\inf}^{*} r T_{10}\right\}\left[\left(B_A^2 - B_B^2\right) I_A^{an} I_B^{an} / \left(B_A^2 I_B^{an} - B_B^2 I_A^{an}\right)\right] \quad (1)$$

* Corresponding author. Address: The Ohio State University, 473 W. 12th Avenue, Room 611C, Columbus, OH 43210, USA. Fax: +1 614 247 7845.
E-mail address: Jay.Zweier@osumc.edu (J.L. Zweier).

1090-7807/$ - see front matter Published by Elsevier Inc.
doi:10.1016/j.jmr.2011.06.030

and

$$C_{O2}^{an} = (1/a_1)\left\{ \left[B_A^2 B_B^2 (I_A^{an} - I_B^{an}) / \left(B_A^2 I_B^{an} - B_B^2 I_A^{an} \right) \right]^{1/2} - a_2 C_R^{an} - a_3 \right\} \quad (2)$$

where C_R^{an} is the concentration of the paramagnetic probe in an analyzed sample, C_{O2}^{an} is the concentration of oxygen in an analyzed sample, $E_{inf}^{*} = E_{inf}[1 - \exp(-T_{EPR}/T_1)]$, T_1 is the proton relaxation time, and E_{inf} is the enhancement at infinite EPR RF power and infinite concentration of the paramagnetic probe. I_A^{an} and I_B^{an} are image intensities of an analyzed sample obtained at B_A and B_B, respectively, and normalized with respect to the EPR-off image. $B_{A(B)}$ is the magnetic component of EPR RF field. A set of parameters that needs to be known prior to the PEDRI experiments are r (relaxivity of the paramagnetic probe), E_{inf} and T_{10} (proton relaxation time in the absence of the probe). Other parameters a_1, a_2, a_3 and α, which denote line broadening due to the presence of oxygen, concentration broadening, intrinsic line width and EPR resonator efficiency, correspondingly, are also needed and should be determined experimentally [18]. a_1, a_2, a_3 are instrument independent parameters of the probe solution and can be measured in separate experiments. α is a characteristic parameter of the instrumental setup and can be measured (for example) by the method of perturbing spheres [19]. However, the resonator efficiency can vary significantly from experiment to experiment and is dependent on the coupling and sample loading of the resonator. The efficiency of the loaded resonator is not only due to the resonator itself, but it is also characteristic of the sample. Sample size and geometry, its dielectric loss and positioning in the resonator control the efficiency α. Changing or even repositioning of the sample will affect α, especially in case of in vivo applications. Therefore, α can be determined in a separate experiment only if the load precisely matches the load of the measured object, which is practically impossible for in vivo applications. In previous research [18], parameters T_{10}, a_1, a_2, a_3 and r were determined at 37 °C in full blood using EPR, NMR and DNP methods.

In order to use formulas (1) and (2), EPR-on image intensities should be normalized with respect to the corresponding EPR-off image, but obtaining a good quality EPR-off image is usually a challenge at 0.02 T due to the low sensitivity of low field MRI. As a result, dividing a PEDRI image by a noisy MRI image gives significant variability in resulting values which can reach infinities at pixels where the MRI image intensities are very low. Therefore, it would be highly desirable to develop an approach to modify existing methods in order to eliminate the necessity for the EPR-off image.

In this report, we propose an improved approach to conduct PEDRI oximetry experiments. Specifically, this involves the inclusion of three reference samples with known concentrations of the probe and oxygen placed together with the sample or animal to be analyzed. This method does not require knowledge of individual values of any parameters defined above, which in the past had to be determined in a separate set of experiments introducing additional experimental error. Another advantage of the proposed method is that the EPR-off image is not required for the calculations of oxygen concentration. With our new approach only two images at different EPR powers are needed. Thus, the PEDRI approach presented in this paper improves the technique by reducing the number of acquisitions needed and, therefore, the total time required for these experiments.

2. Materials and methods

2.1. Chemicals

The water soluble Finland trityl radical was used as a paramagnetic probe [20]. Structure of this probe is shown in Fig. 1. The anaerobic EPR peak-to-peak linewidth is 90 mG.

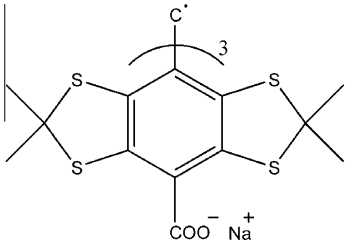

Fig. 1. Structure of the Finland trityl radical.

2.2. Phantom

A phantom was constructed of sealed glass tubes, three tubes of 4 mm and one of 8 mm internal diameter. A diagram of the phantom is shown in Fig. 2A. Three reference tubes were filled with 1 mM (Ref. [1]) or 2 mM (Refs. [2,3]) solutions of the probe. The bigger tube – "analyzed sample" (S) contained 1.5 mM probe solution. These tubes were placed inside a 30 mm diameter plastic tube and outer volume was filled with 60 ml 10% saline (0.09% NaCl) to increase the load of the resonator, simulating an in vivo mouse experiment. Reference solutions 1 and 2 did not contain oxygen; the third solution was equilibrated with air (oxygen concentration 0.24 mM). Two phantom images acquired at two different EPR irradiation powers are shown on Fig. 2B (0.8 W) and C (3.2 W). The calculated maps of the probe and oxygen concentrations are shown on Fig. 2D and E, respectively, with the spatial resolution of 0.5 mm and functional resolution of 0.01 mM for oxygen. MRI signal intensities of the reference tubes, shown on Fig. 2F, differ by 3.1% from the MRI signal intensity of the analyzed sample, i.e. $I_0^1/I_0^{an} \approx 1$ (notation of the symbols is described in Table 2).

2.3. NMR console

Individual parts of the imaging system are controlled by a customized MRRS MR 5000 console (MR Solutions Inc., Surrey, UK), including gradient hardware, the RF system, and the magnet shim coils. The console is used for image acquisition and post-processing.

2.4. Magnet and resonators' assembly

The main vertical magnetic field with a gap of 50 cm between the magnet poles was generated by a water-cooled iron core Resonex 5000/Paradigm resistive magnet (Resonex Corp., Sunnyvale, CA). NMR detection field homogeneity of better than 50 ppm over a sample of size 50 × 40 × 40 cm placed at its isocenter is achieved by a set of 24 active shims. Danfysik MPS 854/SYS 8000 power supply is used to power the magnet. Magnetic field of 0.02 T was used for this study with the maximum of 0.38 T possible with the current setup. Current regulation of the magnetic field relies on the high precision manually adjustable reference voltage. This provides stability better than 0.5 ppm/h of the current and, therefore, of the magnetic field. EPR transmit system is based on a modified Alderman–Grant design resonator with capacitive coupling in combination with a typical solenoidal coil for the NMR channel [21]. EPR radiation power was measured by a power meter (RF Power Analyst, model 4391A), placed between the EPR RF power amplifier and the EPR resonator. The AG resonator used for this work has four capacitive gaps to achieve homogeneity of EPR RF magnetic field. Maximum inhomogeneity observed for this resonator and measured by OE mapping of the uniform sample did not exceed 5% (data not shown).

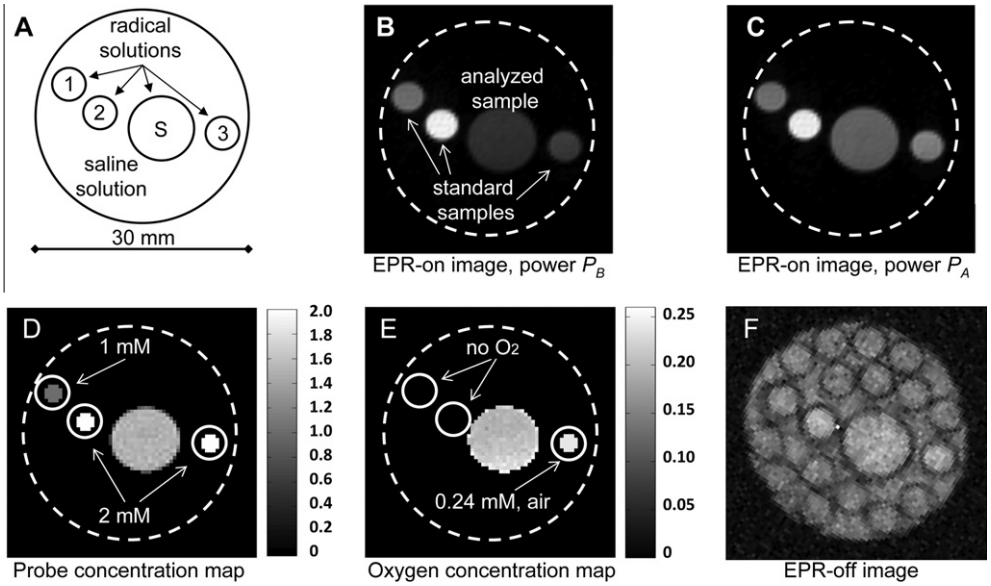

Fig. 2. (A) Schematic representation of the phantom: reference solutions are denoted as 1–3; analyzed sample is denoted as S. (B) Image acquired with EPR power P_A = 0.8 W. Reference samples are denoted as 1–3. All tubes were placed inside a bigger tube, 30 mm diameter, filled with 0.09% NaCl in water. Dashed line schematically shows the location of the tube border, not visible because saline solution surrounding the sample tubes has very small signal intensity compared to the enhanced signals. The MRI acquisition parameters are: TR, 2 s; TE, 30 ms; matrix, 128 × 128; field of view (FOV), 64 × 64 mm; slice thickness, 4 mm; acquisition time, 4.3 min; NMR frequency, 841.5 kHz. EPR irradiation time 4.3 min. (C) Image acquired with EPR power P_B = 3.2 W. (D) Probe concentration map. (E) Oxygen concentration map. (F) MRI image of the phantom. The MRI acquisition parameters are: TR, 2 s; TE, 30 ms; matrix, 128 × 128; field of view (FOV), 64 × 64 mm; slice thickness, 20 mm; acquisition time, 4.3 min; NMR frequency, 841.5 kHz.

2.5. Spin echo sequence and experimental parameters

A standard 2D fast spin echo (FSE) pulse sequence from MR Solutions Inc. was used for fixed-field PEDRI experiments (Fig. 3). The continuous wave (CW) EPR irradiation was turned on about 400 ms before the execution of the FSE pulse sequence and was kept on during the whole *k*-space coverage. Single slice images were typically acquired using the 2D FSE pulse sequence (TR = 2 s, base TE = 30 ms, effective TE = 150 ms, views per segment = 16, slice thickness = 4 mm, FOV = 64 × 64 mm, matrix size = 128 × 128, number of averages = 16, scan time = 4.3 min). MRI frequency was 841.5 kHz. Images were acquired with EPR irradiation at RF = 554 MHz. Incident EPR RF powers were 0.8 and 3.2 W.

The EPR resonance frequency was determined from the equation describing the absorption of microwave energy by a spin system $h\nu = g\beta H$. In this formula h is Planck's constant, ν is the microwave frequency, g is the electron g-factor, β is the Bohr magneton and H is the applied magnetic field. It is important to note that the experimentally determined value of g-factor of the TAM probe differs from that of the free electron by 0.0011. The value is 2.0034; this corresponds to 123.31 mG shift in the magnetic field. The EPR line width of anoxic TAM probe is 90 mG, which is less than the difference between g-factors of the probe and free electron. Therefore, it is possible to miss the point of resonance when performing PEDRI experiments. To avoid this problem, the value of g-factor of the probe has to be accurately measured in advance for the precise matching conditions between the EPR RF frequency and the external magnetic field. Of note, if the matching conditions between the EPR RF frequency and the external magnetic field are not chosen correctly, higher EPR powers are needed to achieve the same enhancement factors as those achieved exactly on the resonance.

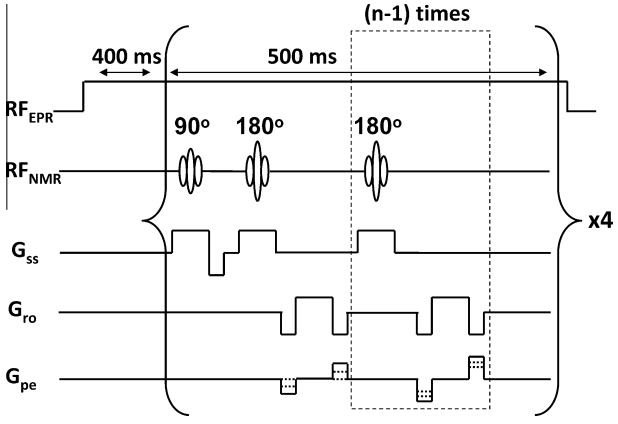

Fig. 3. 2D fast spin echo (FSE) pulse sequence, showing 2 out of 16 180 ° refocusing pulses. Number of echoes per RF excitation, n = 16; the number of RF excitations is 4.

2.6. Theory

Due to the interaction of a paramagnetic probe with water protons, the NMR signal intensity of the latter can be increased by more than an order of magnitude, when the probe is irradiated at the EPR frequency. This enhancement is based on the transfer of polarization from the electron spins to the nuclear spins and can be described in terms of the proton magnetization, M^I, by

$$\frac{M^I - M_0^I}{M_0^I} = -\frac{\gamma_e}{\gamma_n} fkS \tag{3}$$

where M_0^I is the proton magnetization at thermal equilibrium, γ_e and γ_n are the gyromagnetic ratios of electron and nucleus respectively, and their ratio is equal to 658. f is the leakage factor determined as $f = rcT_{10}/(1 + rcT_{10})$, where r is the relaxivity of the probe and T_{10} is the proton relaxation time in the absence of the probe. k is the coupling factor which equals 0.5 for pure dipole electron–nuclear interaction, and c is the concentration of a paramagnetic probe. The saturation factor, S, can be described by

Table 1
Notation of signal intensities obtained in a PEDRI experiment.

Symbol	Definition
I_A^{an}, I_B^{an}	Intensities of EPR-on signal of an analyzed sample, EPR powers P_A, P_B
I_A^1, I_A^2, I_A^3	Intensity of EPR-on signal of reference samples 1–3, EPR power P_A
I_B^1, I_B^2, I_B^3	Intensity of EPR-on signal of reference samples 1–3, EPR power P_B

$$S = -\frac{\gamma_e^2\alpha^2 P T_{1e} T_{2e}}{1+\gamma_e^2\alpha^2 P T_{1e} T_{2e}} \tag{4}$$

where α describes resonator efficiency, P is the incident power, T_{1e} and T_{2e} are the electron relaxation times. The values of T_{1e} and T_{2e} depend on three factors: (1) concentration-broadening of the probe, a_2; (2) broadening due to the presence of oxygen, a_3; and (3) the line width of the probe in the absence of oxygen and at infinite dilution, a_1. This dependence can be summarized by

$$\frac{1}{\gamma_e\sqrt{T_{1e}T_{2e}}} = a_3 + a_2 c_R + a_1 c_{O2} \tag{5}$$

Transient behavior of the proton magnetization can be given by

$$M^I = M_0^I - E_{inf} M_0^I [1-\exp(-T_{EPR}/T_1)] f \frac{\gamma_e^2\alpha^2 P T_{1e} T_{2e}}{1+\gamma_e^2\alpha^2 P T_{1e} T_{2e}} \tag{6}$$

where E_{inf} is the enhancement at infinite EPR power and infinite concentration of the probe. T_{EPR} is the EPR irradiation time, and T_1 is the proton relaxation time.

2.7. Derivation of the approach

Concentration of the probe and oxygen for the three reference samples is denoted as c_R^1–c_R^3 and c_{O2}^1–c_{O2}^3, respectively; c_R^{an} and c_{O2}^{an} are the corresponding concentrations in the analyzed sample. A short description of parameters that can be determined from a PEDRI experiment is given in Table 1. EPR powers are denoted as P_A and P_B; their values are related to the EPR irradiation field, $B_{A(B)}$, as $B_{A(B)} = \alpha\sqrt{P_{A(B)}}$. Table 2 summarizes parameters for the calculation of oxygen and probe concentrations from the PEDRI experiments.

The proton magnetization for individual reference sample and EPR irradiation power P_A can be written as

$$I_A^1 = I_0^1 - I_0^1 \frac{(E_{inf}^* r T_{10}) c_R^1 P_A \alpha^2}{\left(a_3 + a_2 c_R^1 + a_1 c_{O2}^1\right)^2 + P_A\alpha^2} \tag{7}$$

similar expressions can be written for image intensities I_{2A} and I_{3A} of the reference samples 2 and 3. If Eq. (7) is written for an analyzed sample, one more linearly independent equation is necessary to find both concentrations of oxygen and the probe. These two equations were provided by measuring OE at two different EPR powers. By addition of three reference samples it is possible to find both concentrations of oxygen and the probe without the knowledge of parameters listed in Table 2. It is assumed that the product $F = (-E_{inf}^* r T_{10})$, which reflects the relaxation properties of the probe on the solvent is the same for the reference samples as well as for the analyzed sample. Eq. (7), written for each of the three reference samples and two EPR powers, can be transformed into a system of six linearly independent equations

$$I_A^1 = \frac{I_0^1 F c_R^1 P_A \alpha^2}{\left(a_3 + a_2 c_R^1 + a_1 c_{O2}^1\right)^2 + P_A\alpha^2} \tag{8}$$

$$I_B^1 = \frac{I_0^1 F c_R^1 P_B \alpha^2}{\left(a_3 + a_2 c_R^1 + a_1 c_{O2}^1\right)^2 + P_B\alpha^2} \tag{9}$$

Table 2
Description of parameters needed for the calculation of oxygen and probe concentrations.

Symbol	Definition
I_0^{an}	Intensity of EPR-off signal of an analyzed sample
I_0^1, I_0^2, I_0^3	Intensities of EPR-off signal of the reference samples 1–3
α	EPR resonator efficiency, $\mu T/\sqrt{W}$
a_1	Oxygen-dependent line broadening, μT/mM
a_2	Concentration-dependent line broadening, μT/mM
a_3	Intrinsic line width of the probe, μT
E_{inf}	The enhancement at infinite power and at infinite probe concentration
r	Relaxivity of the paramagnetic probe, $mM^{-1}\,s^{-1}$
T_1	Relaxation time of the protons in the presence of the probe, s
T_{10}	Relaxation time of the protons in the absence of the probe, s

$$I_A^2 = \frac{I_0^2 F c_R^2 P_A \alpha^2}{\left(a_3 + a_2 c_R^2 + a_1 c_{O2}^2\right)^2 + P_A\alpha^2} \tag{10}$$

$$I_B^2 = \frac{I_0^2 F c_R^2 P_B \alpha^2}{\left(a_3 + a_2 c_R^2 + a_1 c_{O2}^2\right)^2 + P_B\alpha^2} \tag{11}$$

$$I_A^3 = \frac{I_0^3 F c_R^3 P_A \alpha^2}{\left(a_3 + a_2 c_R^3 + a_1 c_{O2}^3\right)^2 + P_A\alpha^2} \tag{12}$$

$$I_B^3 = \frac{I_0^3 F c_R^3 P_B \alpha^2}{\left(a_3 + a_2 c_R^3 + a_1 c_{O2}^3\right)^2 + P_B\alpha^2} \tag{13}$$

It is important to note that the value of $F_0 = F I_0^1$ does not depend on the EPR-off signal and can be determined from two PEDRI images of any reference sample acquired at different EPR powers, e.g. using Eqs. (8) and (9):

$$F_0 = \frac{I_A^1 I_B^1 (P_A - P_B)}{c_R^1\left(I_B^1 P_A - I_A^1 P_B\right)} \tag{14}$$

Equations for the analyzed sample, written for EPR powers P_A and P_B, respectively, have the form

$$I_A^{an} = \frac{I_0^{an} F c_R^{an} P_A \alpha^2}{\left(a_3 + a_2 c_R^{an} + a_1 c_{O2}^{an}\right)^2 + P_A\alpha^2} \tag{15}$$

$$I_B^{an} = \frac{I_0^{an} F c_R^{an} P_B \alpha^2}{\left(a_3 + a_2 c_R^{an} + a_1 c_{O2}^{an}\right)^2 + P_B\alpha^2} \tag{16}$$

The concentration of the analyzed sample can be found by solving the system of these two equations. Taking into account that $F_0 = F I_0^1$, one can obtain

$$c_R^{an} = \frac{I_0^1}{I_0^{an}} \cdot \frac{I_A^{an} I_B^{an} (P_A - P_B)}{F_0 (I_B^{an} P_A - I_A^{an} P_B)} \tag{17}$$

The concentration depends on the ratio $\frac{I_0^1}{I_0^{an}}$ which, according to the experimental data, can be less or greater than unity by no more than a couple of percent, and therefore, can be neglected. Therefore, final formula for the calculation of c_R^{an} does not contain the intensity of EPR-off signal and has the following form

$$c_R^{an} = \frac{I_A^{an} I_B^{an} (P_A - P_B)}{F_0 (I_B^{an} P_A - I_A^{an} P_B)} \tag{18}$$

Only one of the references is needed to find the probe concentration in an analyzed sample. These calculations are performed at each pixel of the image matrix; and therefore, provide distribution of the paramagnetic material within the sample. For in vivo experiments T_1 and T_2 proton relaxation times can vary resulting

in different MRI signal intensities [22]. It is crucial to design the references with NMR relaxation properties as close as possible to those of the analyzed object. For the cell impermeable TAM probe which stays in blood compartment, care must be taken to ensure that T_1 of the reference sample is similar to that of blood i.e. the ratio I_0^1/I_0^{an} does not significantly deviate from unity.

The concentration of oxygen in the analyzed sample can be derived from Eq. (15). If the probe concentration in reference tubes 2 and 3 is the same, i.e. $c_R^3 = c_R^2$; and reference tubes 1 and 2 do not contain oxygen, $c_{O2}^1 = c_{O2}^2 = 0$, then

$$c_{O2}^{an} = \frac{1}{a_1}\left(\alpha\sqrt{\frac{P_A c_R^{an} I_0^{an} F}{I_A^{an}} - P_A} - a_2 c_R^{an} - a_3\right) \tag{19}$$

Taking into account that $F = F_0/I_0^1$, where the numerator can be found using Eq. (14), the resulting ratio I_0^{an}/I_0^1 can again be approximated to unity, leading to an equation which does not depend on EPR-off signal intensities. By solving the system of three linearly independent Eqs. (8), (10), and (12), and introducing three new variables, i.e. $\gamma_1 = \frac{\alpha}{a_1}, \gamma_2 = \frac{a_2}{a_1}$ and $\gamma_3 = \frac{a_3}{a_1}$, the concentration of oxygen in an analyzed sample can be found as

$$c_{O2}^{an} = \gamma_1\sqrt{\frac{P_A c_R^{an} F_0}{I_A^{an}} - P_A} - \gamma_2 c_R^{an} - \gamma_3 \tag{20}$$

where

$$\gamma_1 = \frac{c_{O2}^3}{(\eta_2 - \eta_3)};\quad \gamma_2 = \frac{(\eta_2 - \eta_1)}{(\eta_2 - \eta_3)}\frac{c_{O2}^3}{(c_R^1 - c_R^2)};\quad \gamma_3 = \frac{c_{O2}^3(\eta_2 c_R^1 - \eta_1 c_R^2)}{(\eta_2 - \eta_3)(c_R^1 - c_R^2)} \tag{21}$$

and

$$\eta_1 = \sqrt{P_A\left(\frac{c_R^1 F_0}{I_A^1} - 1\right)};\quad \eta_2 = \sqrt{P_A\left(\frac{c_R^2 F_0}{I_A^2} - 1\right)};$$
$$\eta_3 = \sqrt{P_A\left(\frac{c_R^2 F_0}{I_A^3} - 1\right)} \tag{22}$$

As a result, the concentration of oxygen as well as the probe in an analyzed sample can be found using intensities of two images, acquired with two known EPR powers P_A and P_B, and knowing corresponding probe and oxygen concentrations in the reference tubes, i.e. c_R^1–c_R^3 and c_{O2}^1–c_{O2}^3.

Similar to the calculation of probe concentration, the equations are applied at each pixel of the images, yielding an oxygen map.

3. Results

For the calculation of oxygen concentration in the analyzed sample two images have been acquired at EPR powers 0.8 and 3.2 W (Fig. 2B and C). Signal to noise ratio was found to be 49 for the lower EPR power and 92 for the higher power with maximum enhancement factor for anoxic 2 mM solution of about 56 (determined as I/I_0). Within each of the tubes MRI signal did not deviate by more than 1.6%.

Distributions of the probe and oxygen within the analyzed sample were calculated using Eqs. (19) and (21): for oxygen 0.23 ± 0.01 mM (actual concentration was 0.24 mM); for the probe 1.49 ± 0.01 mM (actual concentration was 1.5 mM). Corresponding maps are shown in Fig. 2D and E. To increase the accuracy of the calculations, only central pixels inside each of the reference tubes were taken to find averaged signal intensity, excluding "edge" effect. These pixels are shown inside of the circles on the maps (Fig. 2D and E). The concentrations of 1 or 2 mM, shown on the maps, correspond to averaged signal intensities of the reference tubes taken for the calculations. For the analyzed sample, the calculations have been performed for each pixel individually and then the results were plotted as intensity maps. Fig. 4 shows histograms of the distribution of the probe and oxygen concentrations in the analyzed sample.

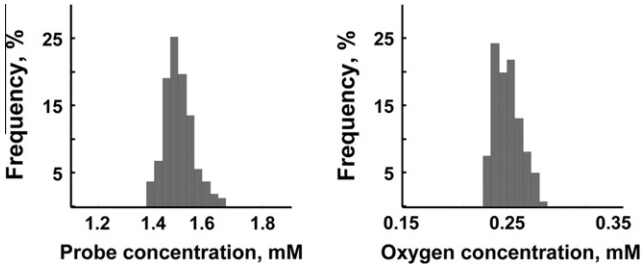

Fig. 4. Histograms of the distribution of the probe and oxygen concentrations in the analyzed sample.

4. Discussion

The enhancement factor (OE) has the following dependence on oxygen and probe concentrations

$$OE \approx \frac{c_R^{an} P_A \alpha^2}{\left(a_1 c_{O2}^{an} + a_2 c_R^{an} + a_3\right)^2 + P_A \alpha^2} \tag{23}$$

where P_A is one of the applied EPR powers. As both oxygen and the probe are paramagnetic, they both affect the enhancement according to the same spin–spin interaction mechanism. However, their effect on OE is different. The difference between these two effects is demonstrated by Eq. (23), where it is shown that oxygen only reduces the enhancement by broadening the EPR line. Probe concentration, on the other hand, increases the enhancement and broadens the EPR signal at the same time. As seen from Fig. 5, power saturation curve (function of enhancement, determined as I/I_0, vs. applied EPR power) is determined by paramagnetic probe concentration and concentration of oxygen. One can see that maximum enhancement factor for anoxic solution with 2 mM probe concentration is about 56. As a result, two linearly independent equations are needed to find both concentrations of oxygen and the probe. Measuring OE at two different EPR powers provides these equations. However, the full set of unknown parameters required to perform the calculations include: a_1, a_2, a_3, α, E_{inf}, r and T_{10} (description is given in Table 2). The intrinsic EPR line width of the probe, a_3, does not depend on experimental settings and can easily be found in an additional anaerobic EPR experiment performed at low probe concentration. Oxygen and concentration induced line broadening, a_1 and a_2, respectively, as well as parameters r and T_{10} may slightly differ with the solvent [18], and therefore, should be determined using reference samples resembling blood or biological tissues as closely as possible. Also, proton relaxation time T_{10} in the absence of a paramagnetic probe can be different within a region of interest, and therefore, cannot be assumed to be uniform [23]. In previous research [16,17], these parameters were determined individually in a separate set of dynamic nuclear polarization (DNP) experiments in whole blood at 37 °C. Using the proposed three reference approach, it is not necessary to know the values of E_{inf}, r, T_{10} and I_0 separately. The product $(I_0 E_{inf} r T_{10})$ can be found in the same PEDRI experiment together with analyzing the sample, using only signal intensities of one of the reference samples.

EPR resonator efficiency α strongly depends on the tuning and coupling of the resonator and can differ significantly with experiment as well as with load. It is usually determined by the method

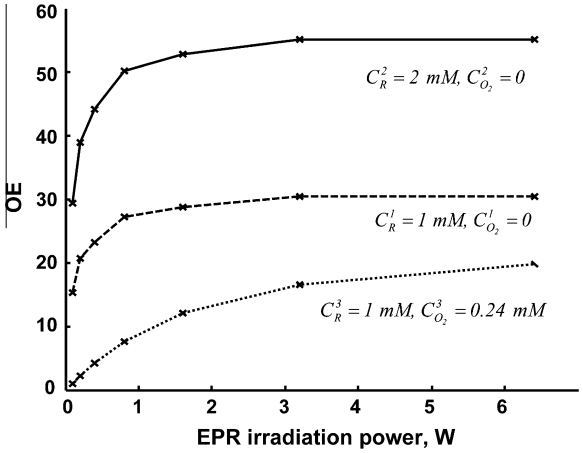

Fig. 5. Enhancement factor (OE), defined as I/I_0, as a function of applied EPR power. Solid line: c_R, 2 mM; dashed and dotted lines: c_R, 1 mM. Samples represented by the solid and dashed lines contained no oxygen. In the third sample oxygen was equilibrated with air. The MRI acquisition parameters are: TR, 2 s; TE, 26 ms; matrix, 128 × 128; field of view (FOV), 64 × 64 mm; slice thickness, 20 mm; acquisition time, 16 s; NMR frequency, 841.5 kHz. EPR irradiation time, 16.4 s; EPR frequency, 554 MHz.

of perturbing spheres [19] without the sample, which may add an additional experimental error to the data when numeral value of α for empty resonator is translated to the loaded resonator. In our approach, the standard samples are placed together with that to be analyzed, so that they experience comparable EPR B_{1e} field during the acquisition. We considered the same α when enhancements of measured and analyzed samples are compared. However, α may be slightly different for the analyzed and reference samples due to EPR RF field inhomogeneity. This inhomogeneity-induced systematic error brings additional error to the functional calculations. The AG resonator used for this work has four capacitive gaps to achieve good homogeneity of EPR RF magnetic field. Inhomogeneity of the resonator as measured by OE mapping of the uniform sample did not exceed 5% (data not shown). But this small error will be introduced into the oxygen measurements in even smaller degree due to the fact that α is present in the Eq. (19) within the square root. Therefore, the results of the calculations are not significantly affected by error in the determination of this parameter, which leads to more reliable data.

EPR powers needed for saturation of the electron system mainly depend on the spectral line width and hyperfine splitting of the spectra of the paramagnetic probe. The narrower the line width, the lower EPR powers are needed for saturation. Nitroxide radicals are also used as paramagnetic functional probes for PEDRI experiments [24,25], however, their broad line width and nitrogen splitting lead to smaller enhancement factors and therefore, to images of lower quality, compared to those obtained with narrow line TAM probes irradiated with the same EPR power. Additionally, oxygen-induced spin–spin line broadening of nitroxides is smaller relative to intrinsic line widths making accurate oxygen measurements with nitroxide probes problematic. TAM probes having intrinsic line width less than 100 mG and oxygen-dependent line broadening of 497 mG/mM are ideal for the oxygen measurements because lower powers are needed to achieve practically useful enhancements at mM probe concentrations. Concentration dependent spin–spin line broadening measured to be 8 mG/mM interferes with oxygen measurements within this concentration range. However, the two-power approach with internal standards automatically takes this effect into consideration. For quantitative analysis, intensity of the images plays a crucial role and determines spatial as well as functional resolution. It has been shown before [17] that the value of SNR should be above 10 to be able to use signal intensities for calculations of functional parameters. In our experiments the powers were 0.8 and 3.2 W with signal to noise ratio measured to be 49 and 92 for the lowest and highest EPR powers, respectively.

The total time needed to perform all the necessary experiments is limited by several factors. For in vivo experiments different stability of the probes and the time course of functional changes in the sample may require fast data acquisitions. The distribution of the probe and the local values of oxygen can also change with time within the body of an animal [15,26]. Therefore, the smaller number of acquisitions, allowed by this approach, can be of great value enabling reduction of the total experimental time.

Advantages of the method include: (1) an EPR-off image is not needed; with only two acquisitions required at two different EPR powers; (2) calculations do not require the knowledge of paramagnetic probe parameters such as a_1, a_2, a_3, α, E_{inf}, r and T_{10}; (3) improved accuracy of oxygen imaging is obtained with less noise and artifacts. Overall these advantages facilitate PEDRI based oximetry allowing more rapid and accurate oxygen imaging.

5. Conclusions

Due to the difficulty of determination of many oximetry related parameters, it is of high importance to design new approaches to optimize the method and increase the accuracy of the calculations.

An approach to perform PEDRI experiments has been developed and tested in in vitro experiments. It has been shown that such parameters as a_1, a_2, a_3, α, E_{inf}, r and T_{10} (Table 2) are not needed for the determination of oxygen in an aqueous sample. This can be achieved in PEDRI experiments by using three reference solutions with known concentrations of a paramagnetic probe and oxygen and placing them inside the resonator together with the sample to be analyzed. Using this approach, only two acquisitions at different EPR powers are needed, significantly reducing total data acquisition time for these experiments. This provides a major advantage of the method, that the EPR-off image acquisition is not required. As a result, division by a very small number is eliminated, leading to smooth and more accurate distributions of the measured probe and oxygen concentrations within a given sample.

Acknowledgments

This work was supported by NIH Grants EB004900 and EB009433. The authors are grateful to Dr. D. Komarov for the valuable help with phantom design and preparation.

References

[1] D.W. Zhao, L. Jiang, E.W. Hahn, R.P. Mason, Comparison of H-1 blood oxygen level-dependent (BOLD) and F-19 MRI to investigate tumor oxygenation, Magnetic Resonance in Medicine 62 (2009) 357–364.
[2] H.J. Halpern, C. Yu, M. Peric, E. Barth, D.J. Grdina, B.A. Teicher, Oxymetry deep in tissues with low-frequency electron-paramagnetic-resonance, Proceedings of the National Academy of Sciences of the United States of America 91 (1994) 13047–13051.
[3] G.L. He, R.A. Shankar, M. Chzhan, A. Samouilov, P. Kuppusamy, J.L. Zweier, Noninvasive measurement of anatomic structure and intraluminal oxygenation in the gastrointestinal tract of living mice with spatial and spectral EPR imaging, Proceedings of the National Academy of Sciences of the United States of America 96 (1999) 4586–4591.
[4] J.L. Zweier, P. Kuppusamy, Electron-paramagnetic resonance measurements of free-radicals in the intact beating heart – a technique for detection and characterization of free-radicals in whole biological tissues, Proceedings of the National Academy of Sciences of the United States of America 85 (1988) 5703–5707.
[5] D.J. Lurie, D.M. Bussell, L.H. Bell, J.R. Mallard, Proton electron double magnetic-resonance imaging of free-radical solutions, Journal of Magnetic Resonance 76 (1988) 366–370.
[6] A.W. Overhauser, Polarization of nuclei in metals, Physical Review 92 (1953) 411–412.

[7] D.J. Lurie, I. Nicholson, J.R. Mallard, Low-field epr measurements by field-cycled dynamic nuclear-polarization, Journal of Magnetic Resonance 95 (1991) 405–409.
[8] A.A. Bobko, I. Dhimitruka, T.D. Eubank, C.B. Marsh, J.L. Zweier, V.V. Khramtsov, Trityl-based EPR probe with enhanced sensitivity to oxygen, Free Radical Biology and Medicine 47 (2009) 654–658.
[9] A.A. Bobko, I. Dhimitruka, J.L. Zweier, V.V. Khramtsov, Trityl radicals as persistent dual function pH and oxygen probes for in vivo electron paramagnetic resonance spectroscopy and imaging: concept and experiment, Journal of the American Chemical Society 129 (2007) 7240.
[10] I. Dhimitruka, O. Grigorieva, J.L. Zweier, V.V. Khramtsov, Synthesis, structure, and EPR characterization of deuterated derivatives of Finland trityl radical, Bioorganic & Medicinal Chemistry Letters 20 (2010) 3946–3949.
[11] B. Driesschaert, N. Charlier, B. Gallez, J. Marchand-Brynaert, Synthesis of two persistent fluorinated tetrathiatriarylmethyl (TAM) radicals for biomedical EPR applications, Bioorganic & Medicinal Chemistry Letters 18 (2008) 4291–4293.
[12] Y.P. Liu, F.A. Villamena, J. Sun, T.Y. Wang, J.L. Zweier, Esterified trityl radicals as intracellular oxygen probes, Free Radical Biology and Medicine 46 (2009) 876–883.
[13] T.J. Reddy, T. Iwama, H.J. Halpern, V.H. Rawal, General synthesis of persistent trityl radicals for EPR imaging of biological systems, Journal of Organic Chemistry 67 (2002) 4635–4639.
[14] S.J. Xia, F.A. Villamena, C.M. Hadad, P. Kuppusamy, Y.B. Li, H. Zhu, J.L. Zweier, Reactivity of molecular oxygen with ethoxycarbonyl derivatives of tetrathiatriarylmethyl radicals, Journal of Organic Chemistry 71 (2006) 7268–7279.
[15] H. Li, Y. Deng, G. He, P. Kuppusamy, D.J. Lurie, J.L. Zweier, Proton electron double resonance imaging of the in vivo distribution and clearance of a triaryl methyl radical in mice, Magnetic Resonance in Medicine 48 (2002) 530–534.
[16] K. Golman, J.S. Petersson, J.H. Ardenkjaer-Larsen, I. Leunbach, L.G. Wistrand, G. Ehnholm, K.C. Liu, Dynamic in vivo oxymetry using Overhauser enhanced MR imaging, Journal of Magnetic Resonance Imaging 12 (2000) 929–938.
[17] M.C. Krishna, S. English, K. Yamada, J. Yoo, R. Murugesan, N. Devasahayam, J.A. Cook, K. Golman, J.H. Ardenkjaer-Larsen, S. Subramanian, J.B. Mitchell, Overhauser enhanced magnetic resonance imaging for tumor oximetry: coregistration of tumor anatomy and tissue oxygen concentration, Proceedings of the National Academy of Sciences of the United States of America 99 (2002) 2216–2221.
[18] J.H. Ardenkjaer-Larsen, I. Laursen, I. Leunbach, G. Ehnholm, L.G. Wistrand, J.S. Petersson, K. Golman, EPR and DNP properties of certain novel single electron contrast agents intended for oximetric imaging, Journal of Magnetic Resonance 133 (1998) 1–12.
[19] J.H. Freed, D.S. Leniart, J.S. Hyde, Theory of saturation and double resonance effects in Esra spectra .3. Rf coherence and line shapes, Journal of Chemical Physics 47 (1967) 2762.
[20] I. Dhimitruka, M. Velayutham, A.A. Bobko, V.V. Khramtsov, F.A. Villamena, C.M. Hadad, J.L. Zweier, Large-scale synthesis of a persistent trityl radical for use in biomedical EPR applications and imaging, Bioorganic & Medicinal Chemistry Letters 17 (2007) 6801–6805.
[21] S. Petryakov, A. Samouilov, M. Roytenberg, H. Li, J.L. Zweier, Modified Alderman–Grant resonator with high-power stability for proton electron double resonance imaging, Magnetic Resonance in Medicine 56 (2006) 654–659.
[22] K.I. Dean, M. Komu, Breast tumor imaging with ultra low field MRI, Magnetic Resonance Imaging 12 (1994) 395–401.
[23] S. Matsumoto, H. Utsumi, T. Aravalluvan, K. Matsumoto, A. Matsumoto, N. Devasahayam, A.L. Sowers, J.B. Mitchell, S. Subramanian, M.C. Krishna, Influence of proton T-1 on oxymetry using Overhauser enhanced magnetic resonance imaging, Magnetic Resonance in Medicine 54 (2005) 213–217.
[24] O.V. Efimova, Z. Sun, S. Petryakov, E. Kesselring, G.L. Caia, D. Johnson, J.L. Zweier, V.V. Khramtsov, A. Samouilov, Variable radio frequency proton–electron double-resonance imaging: application to pH mapping of aqueous samples, Journal of Magnetic Resonance 209 (2011) 227–232.
[25] V.V. Khramtsov, G.L. Caia, K. Shet, E. Kesselring, S. Petryakov, J.L. Zweier, A. Samouilov, Variable field proton–electron double-resonance imaging: application to pH mapping of aqueous samples, Journal of Magnetic Resonance 202 (2010) 267–273.
[26] H. Li, G. He, Y. Deng, P. Kuppusamy, J.L. Zweier, In vivo proton electron double resonance imaging of the distribution and clearance of nitroxide radicals in mice, Magnetic Resonance in Medicine 55 (2006) 669–675.